Journal of Alloys and Compounds 476 (2009) 9–13

Contents lists available at ScienceDirect

Journal of Alloys and Compounds

journal homepage: www.elsevier.com/locate/jallcom

Structure and magnetism of the β-Mn–Co solid-solution phase

O.B. Karlsen[a], A. Kjekshus[b,*], H. Fjellvåg[b], P. Ravindran[b], R. Vidya[b], B.C. Hauback[c]

[a] Department of Physics, University of Oslo, P.O. Box 1048, Blindern, N0316 Oslo, Norway
[b] Centre for Materials Science and Nanotechnology and Department of Chemistry, University of Oslo, P.O. Box 1033, Blindern, N-0315 Oslo, Norway
[c] Institute for Energy Technology, N-2007 Kjeller, Norway

ARTICLE INFO

Article history:
Received 26 June 2008
Received in revised form 27 August 2008
Accepted 3 September 2008
Available online 1 November 2008

Keywords:
Solid-solution
Magnetism
Geometric frustration

ABSTRACT

The crystal structure of the β-$Mn_{1-t}Co_t$ solid-solution phase ($0 \le t \le 0.40$) has been studied with powder neutron (10 and 298 K) and single-crystal X-ray (150 K) diffraction methods. The lattice-constant (a) isotherms at 10, 150, and 298 K go through flat maxima between $t = 0.10$ and 0.25. Up to $t = 0.25$ all Co is found to substitute at the $T1$ ($T1$ = Mn and/or Co) site of the β-Mn crystal structure (position 8c of space group $P4_132$) whereas for $t = 0.40$ also the $T2$ site (position 12d) is partly occupied by Co (some 0.2 Mn + 0.8 Co occupancy of the $T2$ site). The variable positional parameters x (for $T1$) and y (for $T2$) exhibit remarkably small variations with composition (t) and temperature. The present low-temperature powder neutron-diffraction data confirm the earlier finding that the β-$Mn_{1-t}Co_t$ phase does not exhibit conventional co-operative magnetic ordering. However, the appearance of diffuse scattering in the low-temperature diffraction patterns is clearly generated by short-range ordering of magnetic moments, which owing to the atomic arrangement of the β-Mn-type structure becomes geometric frustrated. The temperature dependence of the magnetic susceptibility for β-$Mn_{1-t}Co_t$ is re-measured. Neglecting β-Mn itself (which exhibits virtually temperature-independent paramagnetism), our magnetic susceptibility curves above some 80 K for $t = 0.15$, 0.25, and 0.40 can with good-will be described by the Curie–Weiss relation, indicating antiferromagnetic correlations at low temperatures. However, the thus involved paramagnetic moments and Weiss constants must indeed be stamped as unphysically large.

1. Introduction

Manganese stands out among the metallic elements with its unique crystal structures and odd magnetic properties. The trend-breaking features are associated with the α and β modifications of Mn whereas the properties of the high-temperature (γ and δ) or -pressure (ε) variants largely comply with the pattern traced out along the 3d series. The immediate impression of the crystal structures of α- and β-Mn is that, these phases have more in common with intermetallic compounds than pure elements. This impression is further reinforced by the fact that many proper binary and quaternary intermetallics take the α- and β-Mn-type structural arrangements [1]. (Our interest in this complex element arose through the finding that the low-temperature $Au_{80-v}Cu_vSn_{20}$ phase is isostructural with β-Mn [2].)

Despite frequent studies from 1925 [3,4] onward (the crystal structures of α- and β-Mn were in all essentials solved in 1927–1928 [5,6]) more well-grounded insight into the structural and magnetic properties, phase stability, phase transitions, etc. for the various polymorphs of Mn has only been attained rather recently. Ab initio spin-density-functional computational studies [7,8] have shown that the complex crystal and magnetic structures of α- and β-Mn are the results of the conflicting desires to maximize simultaneously bond strength and magnetic moment. Frustration of antiferromagnetic (AF) exchange interactions leads to a non-collinear arrangement of the moments in α-Mn and a quantum spin-liquid state in β-Mn. Simple AF ground states are found for γ- and δ-Mn whereas the computational results suggest that ε-Mn should be only marginally magnetic at equilibrium. All in all it appears (see the very thorough survey of experimental and theoretical findings in Refs. [7,8]) that the structural and magnetic phase diagram of Mn is well explained by the density-functional approach. However, there are still open questions in relation to the various polymorphs of Mn.

One could expect the following consequences of the substitution of Mn with Co in β-Mn. (i) The spin configurational degeneracy will be removed, resulting in relief of the magnetic frustration. (ii) Replacement of Mn by Co is equivalent to addition of extra electrons to the lattice. If the electron concentration plays an important role in the adoption of the unusual crystal structure and magnetic properties, this can be understood. (iii) Substitution of Mn by a

* Corresponding author at: Department of Chemistry, University of Oslo, P.O. Box 1033, Blindern, N-0315 Oslo, Norway. Tel.: +47 22 85 55 60; fax: +47 22 85 54 41.
E-mail address: arne.kjekshus@kjemi.uio.no (A. Kjekshus).

0925-8388/$ – see front matter © 2008 Published by Elsevier B.V.
doi:10.1016/j.jallcom.2008.09.011

non-magnetic element, e.g., Al slows down the strong AF-correlated spin fluctuations (see, e.g., Refs. [9,10] and references therein) and shifts such systems toward conventional co-operative magnetism. Replacement of Mn by another magnetic atom such as Co may also facilitate long-range magnetic ordering.

The present paper is focused on the structural and magnetic properties of the β-Mn–Co solid-solution phase. Our working hypothesis was that extensive substitution of Co for Mn might release the magnetic frustration and allow deeper exploration of the co-operative magnetic state. However, we were already at the start of the project aware that the spin-liquid state of pure β-Mn probably extends to at least β-$Mn_{0.75}Co_{0.25}$ [11]. On the other hand, the homogeneity range of quenched β-$Mn_{1-t}Co_t$ extends right out to $t \approx 0.43$ [12,13].

We report here on a magnetic susceptibility and powder neutron-diffraction (PND) investigation of β-$Mn_{1-t}Co_t$ ($0 \le t \le 0.40$). Because PND experiences a methodological problem (see Section 3) near to $t = 0.25$, structural data for $t = 0$, 0.25, and 0.40 were also collected with single-crystal X-ray diffraction (SXD). For evaluation of the structural findings it is convenient to regard the SXD-based redetermined structure of β-Mn by Shoemaker et al. [14] as a bench-mark standard.

2. Experimental

Samples with nominal compositions Mn, $Mn_{0.850}Co_{0.150}$, $Mn_{0.750}Co_{0.250}$, and $Mn_{0.600}Co_{0.400}$ (hereafter rounded off to β-$Mn_{0.85}Co_{0.15}$, etc.) were made from 99.99% Mn (Aldrich; crushed flakes, which were treated with a mixture of C_2H_5OH and HCl, rinsed with C_6H_{14}, and finally vacuum dried prior to use) and 99.998% Co (Koch-Light, turning from rods). β-Mn specimens were obtained by heating Mn crushings in sealed, evacuated silica-glass capsules for 1 day at 800 °C and quenching the ampoules into ice water. Specimens of $Mn_{0.85}Co_{0.15}$, $Mn_{0.75}Co_{0.25}$, and $Mn_{0.60}Co_{0.40}$ were prepared and homogenized by melting (at ca. 1350 °C) appropriate amounts of the mixed starting materials in sealed, evacuated silica-glass capsules. The samples were kept 4 h at the maximum temperature and then cooled to room temperature. The heat treatment of additional samples of $Mn_{0.60}Co_{0.40}$ was terminated by quenching from 900 °C. During the entire heating and cooling cycles the sample containers were always surrounded by a protective atmosphere of Ar.

After the initial treatment all samples were carefully crushed and transferred to new silica-glass capsules (evacuated and sealed) and annealed at 1000 °C for 7 days. The heat treatment of the cobalt-containing samples were concluded by controlled cooling from 1000 to 500 °C over 14 days (7 days for some of the samples of $Mn_{0.75}Co_{0.25}$) and then quenched to room temperature.

The samples were checked for homogeneity and characterized by powder X-ray diffraction (PXD) using a Guinier-Hägg camera [Si (a = 543.1065 pm) as internal standard and Cu $K\alpha_1$ (λ = 154.0598 pm) radiation] and/or a Siemens D5000 powder diffractometer (Cu $K\alpha_1$ radiation) with position-calibrated (quartz standard) PSD detector. All samples were homogeneous and except for a small contamination (some 3%) of MnO they were phase pure within the detection limits of PXD. Unit-cell parameters were extracted from the Guinier-Hägg data with the programs SCANPI [15] and CELLKANT [16] and from the powder diffractometer data with standard programs for the system.

PND data were collected with the high-resolution powder neutron diffractometer PUS at the JEEP II reactor, Kjeller, Norway. Cylindrical vanadium sample holders were used. Monochromatic neutrons with wavelength 155.5 pm were obtained from a Ge (5 1 1) focusing monochromator and detected by two 2Θ PSD banks (each covering 20°). Intensity data were collected from $2\Theta = 5$ to 130° in steps of $\Delta(2\Theta) = 0.05°$. The low-angle range $1 \le 2\Theta \le 5°$ was also carefully checked (using improved collimation and prolonged counting time) for reflections of magnetic origin.

Sample temperatures of 298 and 10 or 12 K were obtained by means of a Displex cooling system. A Lake Shore DRC 82C controller was used and the temperature was measured and controlled by means of a silicon diode. Rietveld refinements were performed using the program FULLPROF 98 [17], taking scattering lengths from the library of the program. The profile function used was pseudo-Voigt, with three Gaussian half-width parameters and two Lorentzian coefficients. Isotropic temperature factors were used. Faint reflections originating from the MnO impurity and a slight instrumental defect were removed manually prior to the refinement treatment. The refinements of the PND data were terminated at quite acceptable values for the reliability factors (R_n = 0.057–0.083; R_p = 0.114–0.194; R_{exp} = 0.121–0.191).

Reasonably good quality single crystals were obtained for samples with $t = 0$, 0.25, and 0.40. Prismatic shaped specimens of these [approximate dimensions $0.091 \times 0.043 \times 0.039$ ($0.362 \times 0.258 \times 0.201$ for duplicate run), $0.052 \times 0.0497 \times 0.0498$, and $0.090 \times 0.089 \times 0.062$ mm^3, respectively] were mounted on thin glass fibres on brass pins. Intensity data were collected at 150(2) K with a SMART CCD diffractometer (Siemens) equipped with an Oxford Cryosystems Cryostream Plus device. Mo Kα radiation (71.073 pm) was used and the range of Θ covered was 4.58 to 59.64–61.36° (depending on specimen), limiting indices being −15 (−14) to +15 (−14) for h, k, and l [ca. 17,000 reflections collected (internal R in the range 0.061–0.066), 631–671 of which being independent]. The data were integrated with SAINT [18], corrected for absorption with SADABS [19], and refined using full-matrix least squares against $|F|^2$ with SHELXL [20]. Anisotropic displacement parameters were taken into account and an unequal degree of substitution on the two sites was allowed in the initial refinements of the structures for $t = 0.25$ and 0.40. Based on these findings all Co was fixed at the $T1$ site in the final refinements of β-$Mn_{0.75}Co_{0.25}$. The number of parameters/restrictions was accordingly 10/0 in the final refinements of the structures for $t = 0$ and 0.25 and 14/4 for $t = 0.40$. The refinements of the SXD data were terminated at satisfactory values for the reliability factors ($R1$ = 0.0196–0.0401, $wR2$ = 0.0546–0.0880, Goof = 1.222–1.328).

Magnetic susceptibility measurements were carried out between 4 and 300 K in a field of 1 kOe using a SQUID magnetometer (Magnetic Property Measurement System, Quantum Design). Data were collected on heating with 30–40 mg samples contained in gelatin holders during the measurements.

3. Results

Unit-cell dimension (a) for the present β-$Mn_{1-t}Co_t$ samples are listed in Table 1, and isotherms showing the compositional variation of a at 10/12, 150, and 298 K are shown in Fig. 1. Fig. 1 also includes corresponding room-temperature data available from the literature [13,14], the mutual consistency of which with the present findings being quite good. This is gratifying since the results quoted from the compilation of Pearson [13] refer to chemically analyzed samples. Hence, the close match in Fig. 1 serves to support the use of the nominal compositions as representative measures for the actual compositions of the present samples.

The PND diagrams of β-Mn at 298 and 12 K immediately established lack of conventional co-operative magnetism down to the latter temperature, thus confirming PND findings reported already in 1956 by Kasper and Roberts [21] and later certified in various studies (see, e.g., Refs. [8,9,11,22–25] and references therein). The negative findings indeed ruled out the possibility of "more exotic co-operative arrangements like heli-, cone-, and fan-magnetism" which we hinted at in Ref. [2]. This part of the exercise was of course superfluous, as the literature is unanimous on the lack of conventional co-operative magnetic ordering in β-Mn, but we evidently had desired a personal confirmation. The virtually temperature-independent magnetic susceptibility of β-Mn below 298 K (Fig. 2) is in conformity with the absence of conventional co-operative magnetism, again in accordance with earlier findings [9,22–25].

The PND for data β-$Mn_{0.75}Co_{0.25}$ and β-$Mn_{0.60}Co_{0.40}$ match those for $t = 0$ with regard to lacking evidences for conventional co-operative magnetism. However, in line with the findings for

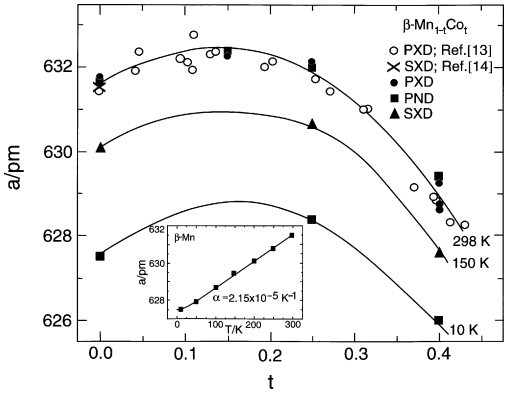

Fig. 1. Isotherms for the compositional variation of the lattice parameter (a) of the β-$Mn_{1-t}Co_t$ phase at 298, 150, and 10 K. Legends to symbols used to distinguish between different experimental techniques are given on the illustration. The inset shows the temperature variation of a for β-Mn.

Table 1
Unit-cell dimensions[a] and positional parameters[b] for the β-$Mn_{1-t}Co_t$[c] phase (space group $P4_132$; *T*1 in position 8*c*, *T*2 in position 12*d*) with e.s.d in parenthesis.

t[d]	*T* (K)	*a* (pm)	*x* for *T*1	*y* for *T*2	Occupancy of *T*1	Method
0.00[e]	298	631.5 (2)	0.0636 (1)	0.2022 (1)	Mn	SXD
0.00	298	631.59 (6)[f]	0.0668 (3)	0.2009 (3)	Mn	PND
0.00[g]	150	629.9 (2)	0.0624 (1)	0.2019 (1)	Mn	SXD
0.00	12	627.47 (6)	0.0650 (3)	0.1989 (3)	Mn	PND
0.15	298	632.19 (2)[h]	0.0659 (6)	0.2022 (2)	0.625 Mn + 0.375 Co[i]	PND
0.25	298	632.04 (5)[j]	0.030 (5)[k]	0.2027 (3)	0.375 Mn + 0.625 Co[i]	PND
0.25	150	630.6 (2)	0.06293 (8)	0.20184 (8)	0.375 Mn + 0.625 Co[i]	SXD
0.25	10	628.4 (2)	0.015 (9)[k]	0.1991 (7)	0.375 Mn + 0.625 Co[i]	PND
0.40	298	629.44 (2)[l]	0.0634 (5)	0.2009 (2)	0.19 Mn + 0.81 Co	PND
0.40	150	627.59 (2)	0.06197 (3)	0.2012 (2)	0.22 Mn + 0.78 Co	SXD
0.40	10	625.98 (2)	0.0640 (5)	0.2003 (2)	0.20 Mn + 0.80 Co	PND
0.40[m]	298	628.82 (3)[n]	0.0631 (5)	0.2024 (3)	0.12 Mn + 0.88 Co	PND

[a] See also Fig. 1.
[b] "Ideal" parameter values; $x = 1/(9+\sqrt{33}) = 0.0678$, $y = (9-\sqrt{33})/16 = 0.2035$, see text.
[c] The powder samples contained some 3% MnO which was corrected prior to the structure refinement.
[d] Nominal compositions, see text.
[e] Data quoted from Ref. [14].
[f] 631.91 (9) pm by PXD.
[g] Essentially identical values for *a*, *x*, and *y* were obtained for the large and smaller crystals; see Section 2.
[h] 632.26 (7) pm by PXD.
[i] Fixed, all Co restrained to the *T*1 site.
[j] 632.07 (9) pm by PXD.
[k] Methodologically induced error, see text.
[l] 629.32 (7) pm by PXD.
[m] Sample quenched from 900 °C.
[n] 628.70 (6) pm by PXD.

β-$Mn_{0.82}Co_{0.18}$ and β-$Mn_{0.75}Co_{0.25}$ reported by Funahashi and Kohara [11] broad diffuse humps appear at low diffraction angles in our 10 K diagrams for β-$Mn_{0.75}Co_{0.25}$ and β-$Mn_{0.60}Co_{0.40}$. Corresponding features were not observed in the 12 K data for pure β-Mn, again confirming findings reported in Ref. [11]. The diffuse diffraction humps are found in the Θ range where the potential magnetic reflections 1 1 0 and 1 1 1 should have occurred (see Ref. [11] for illustrations and further details). From the evolution of the χ (*T*) curves for β-$Mn_{1-t}Co_t$ from $t = 0$ through 0.25–0.40 (Fig. 2) we had somehow expected that the magnetism of the latter sample should carry some of the features ascribed to β-Mn–Al alloys (see, e.g., Refs. [9,10,24–26]).

The variable parameters of the β-Mn-type structure were subjected to Rietveld refinements of the PND data for all samples. All together ten different refinement models were tested, including the alternative space groups $P4_132$ and $P2_13$ and various assumptions concerning the distribution of Mn and Co over the involved sites. Owing to the different sign of the neutron scattering length of Mn and Co, PND is a very sensitive tool to discriminate between distribution alternatives in this case. The conclusions from the Rietveld analyses were that no significant improvements in reliability factors were obtained on turning to the lower symmetric space group and [except for the most substituted ($t = 0.40$) sample] nearly all Co was found to have entered position 8*c* of space group $P4_132$. The final positional and occupancy parameters are listed in Table 1 and corresponding interatomic distances are given in Table 2. In relation to the PND data for $t = 0.25$ it should be noted that average scattering length for 3 Mn and 5 Co randomly distributed over position 8*c* is unfavourably small ($b = 0.339$ fm). This methodological complication is reflected in the unreasonable values obtained for the *x* parameter for this sample at 10 and 298 K, whereas the occupancy parameter for the 8*c* site still can be accurately assessed (Table 1). In order to remedy this defect it was searched for a suitable single crystal of β-$Mn_{0.75}Co_{0.25}$ for SXD examination. Such a specimen was indeed found and the subsequent search for single crystals of β-Mn and β-$Mn_{0.60}Co_{0.40}$ was also successful. SXD data for these specimens (see Section 2) were collected at 150 K and the refinement of which gave the parameter values for *x* and *y* included in Table 1. Note that the positional parameters could be quite precisely determined from SXD data whereas occupancy parameters are less sensitive to the distribution of Co between the two sites. In the final refinement cycles the latter parameters were accordingly fixed at values complying with the PND findings.

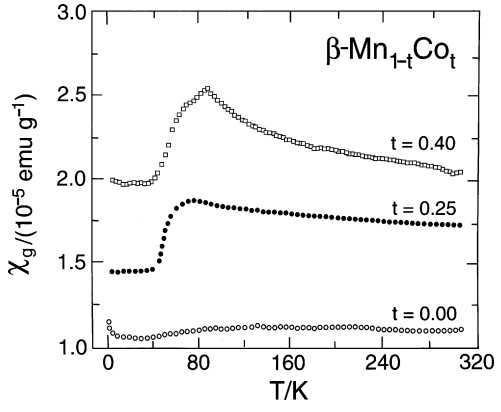

Fig. 2. Temperature variation of the magnetic susceptibility for β-$Mn_{1-t}Co_t$ with $t = 0$, 0.25, and 0.40.

4. Discussion

If the solutes in phases with β-Mn-type structure exclusively enter the 8*c* site, there would occur a natural phase limit at 40% substitution of Co for Mn. Hence, the pronounced site preference of Co for site 8*c* rationalizes why the β-$Mn_{1-t}Co_t$ solid-solution range only extends up to $t \approx 0.43$ [1,12,13]. However, this in turn releases a number of related questions, some of which being formulated and addressed below.

Among the 3*d* series of β-$Mn_{1-t}T_t$ phases those with a *T* element following Mn (viz. *T* = Fe–Zn) show more extended solid-solution ranges than those with *T* = Sc–Cr [1,12,13]. What

Table 2
Bonding interatomic distances (in pm) for the β-$Mn_{1-t}Co_t$ phase at various compositions and temperatures (probable error limits are of the order ±1 pm).

		0				0.15	0.25			0.40			
	"Ideal"[a,e]	T = 298 K SXD[b,e]	T = 298 K PND[e]	T = 150 K SXD[e]	T = 12 K PND[e]	T = 298 K PND[e]	T = 298 K PND[c,e]	T = 150 K SXD[e]	T = 10 K PND[c,e]	T = 298 K PND[e]	T = 150 K SXD[e]	T = 10 K PND[e]	T = 298 K PND[d,e]
$T1$–$T1$ × 3	234.7	236.4	235.1	236.3	234.3	235.7		236.3		235.7	235.6	234.1	235.6
$T1$–$T2$ × 3	260.6	257.6	259.6	256.1	257.9	259.9		256.9		257.3	255.1	256.7	256.0
$T1$–$T2$ × 3	260.6	263.4	261.2	263.6	259.0	261.7		263.3		261.7	262.4	259.3	262.9
$T1$–$T2$ × 3	268.7	268.0	268.0	267.1	265.6	268.5		267.4		266.8	265.9	265.2	266.8
$T2$–$T1$ × 2	260.6	257.6	259.6	256.1	257.9	259.9		256.9		257.3	255.1	256.7	256.0
$T2$–$T1$ × 2	260.6	263.4	261.2	263.6	259.0	261.7		263.3		261.7	262.4	259.3	262.9
$T2$–$T1$ × 2	268.7	268.0	268.0	267.1	265.6	268.5		267.4		266.8	265.9	265.2	266.8
$T2$–$T2$ × 4	265.4	264.6	263.8	263.7	260.9	264.9	265.1	264.0	261.4	262.9	262.3	261.1	263.6
$T2$–$T2$ × 2	265.4	267.2	269.3	267.1	270.7	267.6	266.8	267.5	270.8	268.4	267.2	267.9	265.9
$T2$–$T2$ × 2	326.5	327.1	327.7	326.4	326.6	327.4	327.1	326.8	327.0	326.6	325.5	325.1	325.6

[a] Assuming a = 631.51 pm from Ref. [14].
[b] Based on structural parameters from Ref. [14].
[c] Interatomic distances which involve $T1$ are burdened with methodological problem (see text).
[d] Sample quenched from 900 °C.
[e] Method.

do these apparently trivial observations convey? The size of Mn relative to T is surely involved (see, e.g., Fig. 6 in Ref. [2]) but size is certainly not the one-and-only factor. Electronic characteristics of T obviously also contribute to stabilization/destabilization of β-$Mn_{1-t}T_t$ relative to α-$Mn_{1-t}T_t$ (see Refs. [7,8] and references therein) and other involved phases in the Mn–T systems [12]. As a supplementary detail in this connection, it may be mentioned that the β-$Mn_{1-t}Co_t$ phase has the most extended homogeneity range among the β-$Mn_{1-t}T_t$ phases (followed by β-$Mn_{1-t}Fe_t$ ($0 \le t < \sim 0.32$) and β-$Mn_{1-t}Ni_t$ ($0 \le t < \sim 0.26$); note that the pattern can differ when non-transition-metal solutes are involved (see, e.g., β-$Mn_{1-t}Al_t$ ($0 \le t < \sim 0.40$) where most of the Al is found to enter the $T2$ site (position 12d) [9,10]).

A closely related question is why the site preference for 8c is approximate and not exact. An unobligatory answer could be to maintain that this is a reflection of the universal observation that some solid-solution phases exhibit broad homogeneity regions and other rule in rather narrow fields. A comparative neutron-diffraction study [27] of the β-$Mn_{1-t}T_t$ phases with T = Fe, Co, and Ni shows that at a substitution level of $t \approx 0.1$ almost 90% of the solute enter the $T1$ site. For β-$Mn_{1-t}Co_t$ in particular it was discovered that long-range ordering of Mn and Co within the $T1$ site takes place below 500 K. The decisive factors are again the energetics of the phase in question in relation to the energetics of all neighboring phases. For β-$Mn_{1-t}T_t$ phases it would of course be of particular interest to know the evolution in energetics on substitution of both the $T1$ and $T2$ sites by various T solvents. (Certain aspects of this complex problem can hopefully be explored experimentally and/or theoretically.)

A characteristic feature of the composition variation in the unit cell of β-$Mn_{1-t}Co_t$ (Fig. 1) is that $a(t)$ goes through a flat maximum somewhere between t = 0.10 and 0.25. The initial increase in the $a(t)$ isotherms can be rationalized by accepting that Co has a somewhat larger size than the Mn1 host it replaces (see Fig. 6 in Ref. [2]). The composition dependence of the averages for the 12 Mn1–Mn and 14 Mn2–Mn bond distances at 298, 150, and 10 K (Table 2) lends support to such an inference. (Note that the averages are less infested with random errors than the individual distances.)

What could then cause $a(t)$ to decrease again? One feature which clearly comes into the picture is the dispersing of the substituting Co atoms on the 8c site as well as the larger sized 12d site. The actual observations for β-$Mn_{0.60}Co_{0.40}$ (see Table 1) suggest that the observed change in the occupancy pattern between the two sites could be a significant contributing factor to the more rapid decline of $a(t)$ toward t = 0.40. In general, $a(t)$ is determined by not only the distribution of Mn and Co between the $T1$ and $T2$ sites but also by the short- and long-range orders within the two sites. In this connection we draw attention to the composition variation of the long-range order parameter for the corresponding β-$Mn_{1-t}Fe_t$ phase deduced from ^{57}Fe Mössbauer spectroscopy [28]. This study shows that with increasing Fe content, the long-range-order parameter for the Fe distribution follows a dependence which somewhat resembles $a(t)$ in Fig. 1.

Another characteristic feature, which the β-$Mn_{1-t}Co_t$ phase has in common with isostructural phases, is the comparative constancy of the positional parameters x and y and their closeness rather than full conformity to the "ideal" (see Refs. [2,29]) values for these parameters. As evident from Table 2 there is indeed some variation in the bonding interatomic distances with composition and temperature. The overall trend is that the bond distances are shortest at the highest substitution level (t = 0.40) and lowest temperature (10 K).

A detailed comparison of the bond distances corresponding to the "ideal" [2,29] values of x and y with those actually observed for the β-$Mn_{1-t}Co_t$ phase (Table 2) leads to the conclusion that there is not a geometric (viz. symmetry) factor which prevents the structure from accepting the "ideal" demands. This finding appears to be a logical consequence of the somewhat unspecific constraint which crops up in the formulation of the ideality criterion [2,29]: *as many as possible of the shorter $T1$–$T2$ distances are required to be equal and similarly for the six shortest $T1$–$T2$ distances*.

The recent comprehensive density-functional theoretical exploration of allotropes of manganese [7,8] concluded that the complex crystal structure and frustrated magnetism of β-Mn are the results of conflicting desires to maximize simultaneously bond strength and magnetic moment. The computational efforts moreover established that the ambient pressure polymorphs α, β, γ, and δ are close in energy which inter alia has allowed the many studies of β-Mn as a metastable phase at and below room temperature. That is all very well, but it is more interesting to trace features which make the β-Mn-type structure with its differently sized Mn atoms so favourable. We intend to pursue this problem by theoretical examination of the chemical bonding in β-$Mn_{1-t}T_t$ phases.

Given the β-Mn-type structural arrangement the lacking conventional co-operative magnetism of β-$Mn_{1-t}Co_t$ might at first be regarded as a trivial prolongation of the geometrically frustrated situation of the magnetic moments at t = 0. However, the introduction of Co into the picture has altered two magnetic distinguishing marks compared to the prestine phase. (i) The diffuse scattering of magnetic origin which appears in the PND diagrams

for $t > 0$ has no counterpart for $t = 0$. (ii) The virtually temperature independent paramagnetic susceptibility characteristic for pure β-Mn develops into a more and more Curie–Weiss-like relationship for $t > 0$. These tendencies indicate that magnetic traits of character become enhanced on the Co-for-Mn substitution. However, the non-observation of long-range magnetic ordering shows that the spin-configurational degeneracy is not removed by the Co-for-Mn substitution. This implies that the magnetic frustration arising from the corner-shared triangular sub-units created by Mn2 are not appreciably affected by the Co substitution. This is consistent with the experimental fact that Co predominantly prefers to occupy the Mn1 site, and could in turn provide another reason for why the solubility of Co in β-Mn is limited to ∼40 at.%. On the other hand, if one accepts the postulated [8] decisive role of regular $Mn1Mn2_3$ tetrahedra for the structure and other properties of β-Mn as a reference frame, the frustration would then rather be consequence of the perturbation of the majority Mn2 atoms by the intruded Co atoms on the Mn1 sublattice. According to this picture long-range magnetic ordering facilitated by Co substitution breaks the tetrahedral units and hence lifts the degeneracy of the spin configuration. As the frustration of the spins arising from corner-shared Mn2 triangles should not be influenced noticeably by Co-for-Mn substitution, the long-range magnetic ordering would remain suppressed.

We have for the time being no plausible explanation(s) to offer for the gradually more and more Curie–Weiss-like relationship for $t > 0$ (note with unphysically large paramagnetic moments and Weiss constants), but we intend to pursue also these features by computational density-functional means.

References

[1] P. Villars, L.D. Calvert, Pearson's Handbook of Crystallographic Data for Intermetallic Phases, vols. 1–3, American Society of Metals, Metals Parak, Ohio, 1985.
[2] O.B. Karlsen, A. Kjekshus, C. Rømming, E. Røst, Acta Chem. Scand. 46 (1992) 1076.
[3] A.J. Bradley, Philos. Mag. 50 (1925) 1018.
[4] A. Westgren, G. Phragmen, Z. Phys. 33 (1925) 77.
[5] A.J. Bradley, J. Thewlis, Proc. R. Soc. Lond. A 115 (1927) 456.
[6] G.D. Preston, Philos. Mag. 5 (1928) 1198;
G.D. Preston, Philos. Mag. 5 (1928) 1207.
[7] D. Hobbs, J. Hafner, D. Spišák, Phys. Rev. B 68 (2003) 014407.
[8] J. Hafner, D. Hobbs, Phys. Rev. B 68 (2003) 014408.
[9] H. Nakamura, K. Yoshimoto, M. Shiga, M. Nishi, K. Kakurai, J. Phys.: Condens. Matter 9 (1997) 4705.
[10] J.R. Stewart, R. Cywinski, Phys. Rev. B 59 (1999) 4305;
J.R. Stewart, R. Cywinski, J. Magn. Magn. Mater. 272–276 (2004) 676.
[11] S. Funahashi, T. Kohara, J. Appl. Phys. 55 (1984) 2048.
[12] T.B. Massalski, J.L. Murray, L.H. Bennett, H. Baker, L. Kacprzak (Eds.), Binary Alloy Phase Diagrams, American Society for Metals, Metals Park, Ohio, 1986.
[13] W.B. Pearson, Handbook of Lattice Spacings and Structures of Metals and Alloys, vol. 1, Pergamon, London, 1958, p. 509.
[14] C.B. Shoemaker, D.P. Shoemaker, T.E. Hopkins, S. Yindepit, Acta Crystallogr. Sect. B 34 (1978) 3573.
[15] P.-E. Werner, The Computer Program SCANPI, Institute of Inorganic Chemistry, University of Stockholm, Stockholm, Sweden, 1981.
[16] N.O. Ersson, Program CELLKANT, Chemical Institute, Uppsala University, Uppsala, Sweden, 1981.
[17] J. Rodriguez-Carvajal, Program FULLPROOF 98 Version 02, ILL, Grenoble, France, 1998.
[18] Area-Detector Integration Software V7.12A, Bruker-Nonius Inc., Madison, WI, 2004.
[19] Bruker-Nonius Inc., Madison, WI, 2004.
[20] G.M. Sheldrick, SHELXL97—Program for Crystal Structure Refinement, Institut für Anorganische Chemie der Universität Göttingen, Germany, 1997.
[21] J.S. Kasper, B.W. Roberts, Phys. Rev. 101 (1956) 537.
[22] Y. Masuda, K. Asayama, S. Kobayashi, J. Itoh, J. Phys. Soc. Jpn. 19 (1964) 460.
[23] T. Hori, J. Phys. Soc. Jpn. 38 (1975) 1780.
[24] M. Shiga, H. Nakamura, M. Nishi, K. Kakurai, J. Phys. Soc. Jpn. 63 (1994) 1656.
[25] Y. Kohori, Y. Iwamoto, Y. Muro, T. Kohara, Physica B 237/238 (1997) 455.
[26] J.R. Steward, A.D. Hillier, S.H. Kilcoyne, P. Manuel, M.T.F. Telling, R. Cywinski, J. Magn. Magn. Mater. 177–181 (1998) 602.
[27] H. Oyamatsu, Y. Nakai, N. Kunitomi, J. Phys. Soc. Jpn. 58 (1989) 3606.
[28] A.S. Vinogradova, A.S. Ilyushin, I.A. Nikanorova, V.S. Rusakov, Fiz. Tverd, Tela (St. Petersburg) 39 (1997) 1437;
A.S. Vinogradova, A.S. Ilyushin, I.A. Nikanorova, V.S. Rusakov, Engl. Transl. Phys. Solid State 39 (1997) 1276.
[29] M.O. O'Keeffe, S. Andersson, Acta Crystallogr. Sect. A 33 (1977) 914.